Structural, magnetic, and electrical properties of sol-gel derived cobalt ferrite nanoparticles

A. Hossain, × M S I Sarker, × M K R Khan, F A Khan, × M Kamruzzaman, × M M Rahman

▶ **To cite this version:**

HAL Id: hal-02366403
https://amu.hal.science/hal-02366403

Submitted on 15 Nov 2019

CrossMark

Structural, magnetic, and electrical properties of sol–gel derived cobalt ferrite nanoparticles

A. Hossain[1] · M. S. I. Sarker[1] · M. K. R. Khan[1] · F. A. Khan[2] · M. Kamruzzaman[3] · M. M. Rahman[1]

Abstract

This work reports the synthesis and studies of semi-soft ferrimagnetic $CoFe_2O_4$ nanoparticles using sol–gel method. The X-ray diffraction patterns confirm the formation of cubic spinel $CoFe_2O_4$ nanoparticles. The average crystallite size was found from XRD data is about 30 nm. The high resolution transmission electron microscopy analysis shows that nanoparticles are highly crystalline. The magnetic properties reveal that the particles are ferrimagnetically ordered soft magnetic materials with coercive field of 620 Oe and saturation magnetization $M_s = 60$ emug^{-1}. The higher value of saturation magnetization is due to the ordered single-domains magnetic nanoparticles and lower magnitude of coercivity is attributed to the decrease of inter-particle interactions and magneto-elastic anisotropy. The value of remanence ratio $R < 0.5$ is responsible for magnetostatic interactions of the particles. The nanoparticles possess low values of dielectric constant which decreased with increasing frequency. The low dielectric constant makes the nanoparticles as a promising candidate for high frequency magnetic devices.

1 Introduction

Magnetic metals and metal oxides are very important in materials science and engineering due to their wide range of application and outstanding properties. Soft magnetic materials constitute an important class of engineering materials [1, 2] as they can be easily magnetized and demagnetized under a small external field. Their magnetic properties are important for applications involving power generation and distribution, actuator, magnetic shielding, data storage, and microwave communication.

Co based alloy nanoparticles (NPs) as well as its bulk counterpart such as FeCo, CoNi, etc., are important class of materials owing to their interesting properties like low coercivity and high saturation magnetization [3]. Moreover, $CoFe_2O_4$ NPs has great importance due to its unique physical properties such as high Curie temperature, moderate saturation magnetization, large magneto crystalline

anisotropy, high magneto-strictive coefficient, excellent chemical stability and mechanical hardness [4]. In addition to that, $CoFe_2O_4$ NPs shows high electrical resistance and low dielectric constant. For these properties $CoFe_2O_4$ is technologically important and suitable for high density magnetic recording media [5], ferrofluid technology, bio-medicine, magnetic resonance imaging, biosensors, magnetic hyperthermia based therapy, data storage, magnetic refrigerators and microwave devices [6].

Dielectric ferrites have a high conduction grains separated by poorly conducting grain boundaries [7, 8]. These grain and grain boundaries affect on conductivity due to the hopping of ions with applied external electric field. The above mentioned properties of spinel $CoFe_2O_4$ NPs are affected by composition and microstructure due to the octahedral and tetrahedral occupancy of cations Fe^{3+} and Co^{2+} in the lattice sites. Moreover, the size and shape of the NPs also affects to magnetic properties. Therefore, the control of the size and shape of the NPs are quite important.

Different chemical routes have been used to synthesis the magnetic NPs such as sol–gel method [9], micro emulsion [10], co-precipitation method [11], polyol reduction method [12] etc. Among these methods, sol–gel is an excellent chemical route for obtaining fine nanocrystalline and homogeneous powder because it is simple, environment friendly, cost effective and low temperature operation.

✉ M. S. I. Sarker
  samiul-phy@ru.ac.bd

[1] Department of Physics, University of Rajshahi, Rajshahi 6205, Bangladesh

[2] Department of Physics, Bangladesh University of Engineering and Technology, Dhaka 1000, Bangladesh

[3] Department of Physics, Begum Rokeya University, Rangpur 5400, Bangladesh

Despite several researches on $CoFe_2O_4$, but the systematic studies are rarely reported. In this research, we report a simple process to synthesis $CoFe_2O_4$ NPs using sol–gel method in which ferric (III) chloride and cobalt (II) chloride were used as a precursors and citric acid was used as a capping agent. The crystal structure, surface morphologies, as well as the magnetic and electrical properties of the as synthesized NPs were investigated.

2 Experimental procedure

The experimental sample was prepared by conventional sol–gel method. Stoichiometric amounts of 0.596 g $CoCl_2 \cdot 6H_2O$ (97%: Merck), 0.408 g $FeCl_3$ (98%: Merck) dissolved in 100 ml distilled water and a few drops of concentrated nitric acid were also added to prevent hydrolysis. Citric acid and a few ml of dimethylamine were subsequently added to the solution, which was then magnetically stirred at 70 °C for 2 h and evaporated at 100 °C to form a gel. The gel mixture was dried at 150 °C for 12 h and the resulting powder was decomposed in air and heated in a furnace at 250 °C for 3 h. Finally, the powder samples were ground thoroughly using an agate mortar pestle and heat treated further at 600 °C for 4 h inside a furnace at ambient temperature.

X-ray diffraction (XRD) analysis was performed using Rigaku Smart Lab X-ray diffractometer, operating at a voltage of 45 kV and current of 150 mA with Cu–k_α ($\lambda = 1.54184$ Å) radiation to identify the phases and to determine lattice parameter. The morphological studies were performed by field emission scanning electron microscopy (FE-SEM) with accelerating voltage 5 keV (Philips XL30 FEG) and with a high resolution transmission electron microscopy (HRTEM) with 200 keV (Philips FEG TEM CM200). The thermal analysis was carried out from thermogravimetric analysis (TGA) and differential thermal analysis (DTA) in a controlled atmosphere. The TGA and DTA were performed (Pyris Series STA-8000 Perkin Elmer) on synthesized NPs from 30 to 900 °C to obtain its phase transition temperature, thermal stability and crystalline formation by observing weight loss and heat flow with the increasing of temperature. During TGA and DTA analysis, sample was heated in a tubular electrical furnace under a constant flow of nitrogen gas. The molecular bond in the NPs and the presence of functional group with associated molecular vibration were determined with wavenumber in the range of 225–4000 cm^{-1} with a high resolution Fourier transform infrared radiation (FTIR) spectrometer (Perkin Elmer 100). The resolution of FTIR spectroscopy was 1 cm^{-1} (KBr was used with synthesized NPs as annealing materials in FTIR investigation). The magnetic measurements were carried out using a vibrating sample magnetometer (VSM) at room temperature (using BRUKER type magnet serial no.

811336 and PAR Lock-in Amplifier 5210). The ac electrical measurements were done in a Wayne Kerr 6500B impedance analyzer with a frequency range 100 Hz–10 MHz at different temperatures. A disk shaped sample having 14 mm in diameter and 3 mm in thickness was prepared to determine electrical properties. The surfaces of the disk were polished roughly and then coated with silver paste on both sides for the measurements.

3 Results and discussion

3.1 Structural characterization

Figure 1 shows the XRD patterns of the as synthesized powder sample annealed in air at 600 °C. The observed peaks (220), (311), (222) (400), (422), (511), (440) and (533) can be indexed from the Joint Committee Powder Diffraction Standard (JCPDS) card for spinel $CoFe_2O_4$ cubic structure (No. 22-1086) [11]. Besides, the peaks around 44° and 65° corresponding to the crystal planes (110) and (200) indicate a small amount of FeCo alloy formation in the composition [4, 11]. The space group of $CoFe_2O_4$ is Fd-3m and the calculated lattice parameter is found to be 8.403 Å [11]. XRD pattern also confirms no other unreacted species or impure phase is detected in the sample. The average crystallite size was determined from XRD peak broadening using the Debye–Scherrer formula [13]. $D = K_\alpha \lambda / \beta \cos \theta$, where, λ is the wavelength of the X-ray radiation, K_α is a constant (0.94), β is the full width at half maximum in radian and θ is
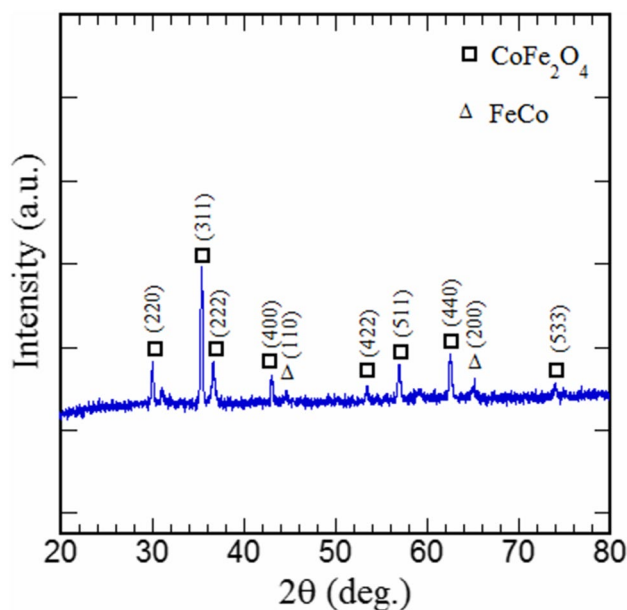

Fig. 1 X-ray diffraction patterns of the as synthesized materials annealed at 600 °C

the diffracting angle. The average crystallite size was found to be 30 nm. In the spinel structure, the cations Co^{2+} and Fe^{3+} may occupy two different sites, i.e., octahedral and tetrahedral sites within the lattice structure. The actual cation distribution is characterized by degree of inversion, which is the fraction of divalent cations occupied in octahedral sites [14]. The divalent Co atoms shared both octahedral and tetrahedral sites in $CoFe_2O_4$ NPs. Therefore, in the microstructural state of the as synthesized spinel $CoFe_2O_4$, it is assumed Co atoms may occupy the same tetrahedral and octahedral sites.

3.2 Surface morphologies

Figure 2 shows the scanning electron microscopy (SEM), transmission electron microscopy (TEM) and high resolution TEM images of the as synthesized cobalt ferrite NPs. It is seen from the SEM micrograph in Fig. 2a that the synthesized particles are formed as octahedron and tetrahedron nanometer in size with some micrometer phases. The microstructure of synthesized NPs reveals the crystallites are perfectly ordered with porous structure. The porosity was determined using the empirical formula: $P = 1 - (\rho_m/\rho_x)$, where, ρ_m and ρ_x are measured density and X-ray density of the NPs, respectively [10]. The porosity of the NPs is about 17.5%. It can be seen from TEM image in Fig. 2b that the sizes of the particle is in the range of 30–40 nm, which corresponds XRD data. The high resolution TEM images shown in Fig. 2c, d indicate the NPs are highly ordered and crystalline. Furthermore, the particles are assumed to be single domain.

3.3 Thermal analysis

The thermal stability $CoFe_2O_4$ nanomaterials was investigated by TG-DTA from room temperature to 900 °C with increasing temperature 20 °C/min. Figure 3 shows the relative weight variation during the heating of the samples in air. It is seen from Fig. 3 that the first weight loss of 5% is associated to an endothermic peak and is related to water loss, which occurs in two steps, dehydration and then loss of adsorbed water until 250 °C [15]. The second weight loss between 20 to 60% is related to a high exothermic peak as well as decarbonation of the samples [15, 16]. The decarbonation has lasted up to the temperatures 500 °C (Fig. 3a). Above that temperature (around 600 °C) the samples has presumably entered in an ordered state. The differential thermal analysis (DTA) for the synthesized nanomaterials in Fig. 3b has shown some exothermic peaks around 273 and 340 °C temperatures, which is attributed to the formation

Fig. 2 a SEM microstructure, **b** TEM image, and **c, d** are HRTEM images of the synthesized NPs annealed at 600 °C
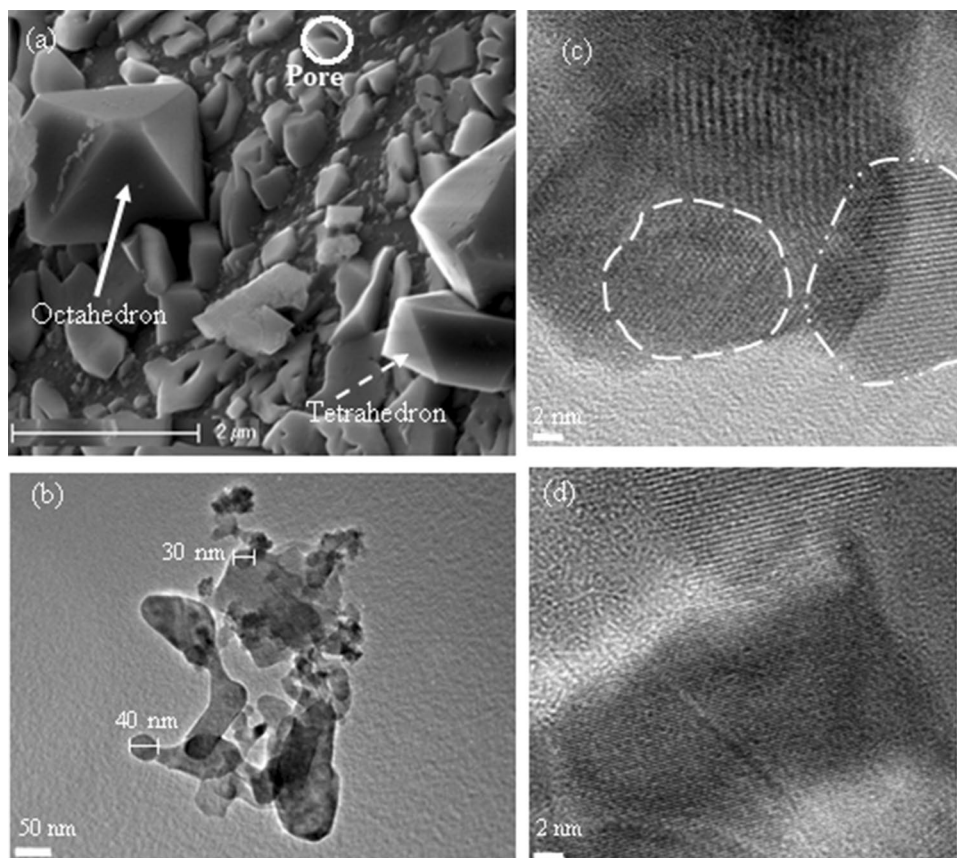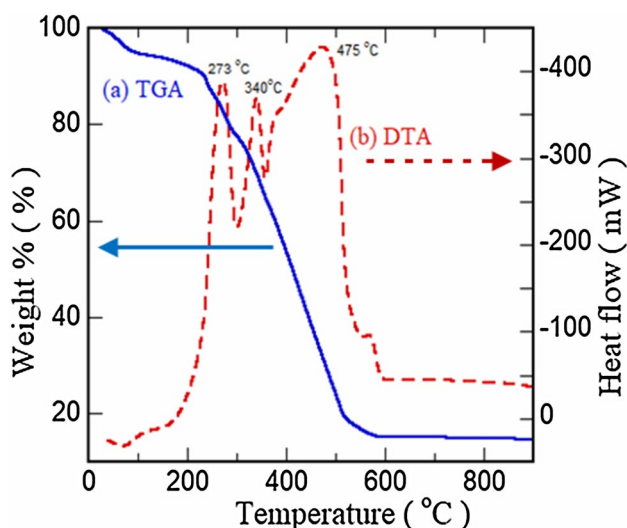
Fig. 3 **a** TGA (solid line) and **b** DTA (dashed line) curves of the as synthesized $CoFe_2O_4$ nanomaterials

of crystalline phases. The exothermic peak at 475 °C temperature is due to the rearrangement of the crystal lattice. Both the TGA and DTA curves show the signature of good quality samples.

3.4 FTIR spectra analysis

The surface chemical properties of the NPs were investigated using FTIR spectroscopy with high resolution of 1 cm^{-1}. Figure 4 shows the FTIR spectra of the $CoFe_2O_4$ NPs observed in the range from 225 to 4000 cm^{-1}. The vibrational spectra of the absorption band were 385.56 and 487.15 cm^{-1}due to vibration of metal oxide such as Fe–O and Co–O which is consistent with ferrite for the octahedral site [17]. The intense peak at 588.48 cm^{-1} in the FTIR spectrum was attributed to the Co–O stretching vibration
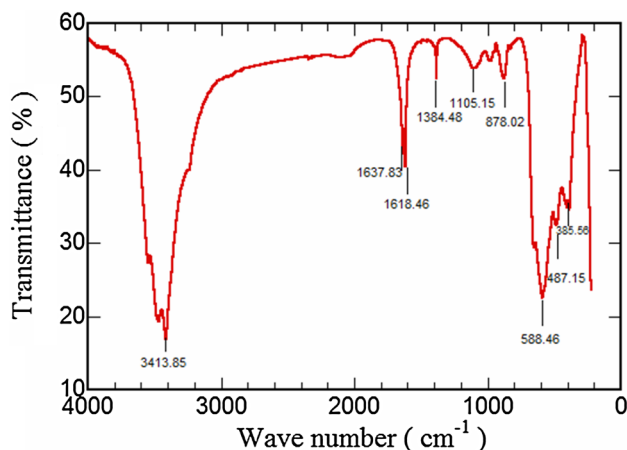

Fig. 4 FTIR spectra of the as synthesized NPs

indicates tetrahedral site in the spinel structure [16]. Thus, the cations of the NPs randomly occupied in octahedral and tetrahedral sites [10, 18–20]. The other peaks such as 1637.83 and 1618.46 cm^{-1} were represented the N–H bending vibration and 1384.48 cm^{-1} was due to bending vibration of C–H group. Moreover, the peaks 1105.15 and 878.02 cm^{-1} were shown in Fig. 4 for C–N, N–H stretching vibration [17]. The peak 3413.45 cm^{-1} was due to stretching vibration of O–H group, which indicate the presence of moisture in the molecule.

3.5 Magnetic properties

It is important to study the magnetic properties of $CoFe_2O_4$ NPs due to the mixed valence state of Co. The anisotropic behavior of Co^{2+} ions is responsible to change the magnetic properties of the synthesized $CoFe_2O_4$ NPs. Figure 5 shows the magnetization, M as a function of magnetic field, H at room temperature in the range of − 7 to 7 kOe of the as synthesized spinel $CoFe_2O_4$ NPs. The NPs behaves as a soft ferrimagnet with coercivity, H_c = 620 Oe and saturation magnetization, M_s = 60 emug^{-1} at room temperature. It is observed that the saturation magnetization of $CoFe_2O_4$ is higher than the values obtained by modified wet chemical process and hydrothermal process [22, 23]. The higher saturation magnetization reported in this study is attributed to the perfectly ordered single-domains magnetic NPs [3]. On the other hand, the lower coercivity is found due to the decrease of interparticle interactions and magneto-elastic anisotropy [22]. The retentivity of the magnetic nanomaterials is equal to M_r = 13.5 emug^{-1} as shown in Fig. 5 and the remanence ratio ($R = M_r/M_s$) of the NPs is 0.22. The
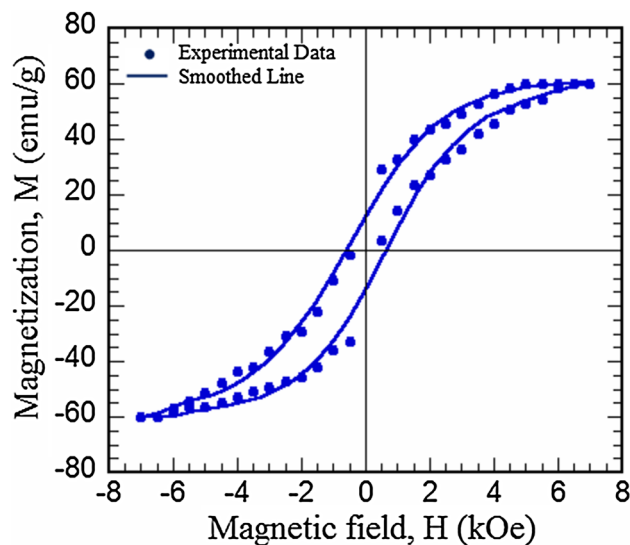

Fig. 5 The magnetic hysteresis loop of the cobalt ferrite NPs measured at room temperature

existence or absence of the different types of inter grain group exchanges is determined by the amount of R that varies from 0 to 1 [24]. The variation of remanence ratio with the particle size can be explained based on domain structure, crystal size and anisotropy of the crystal [25]. More explicitly, the magnetic properties of ferrite NPs depend on the preparation method. For example, it is reported that 16 nm cobalt ferrite NPs made by co-precipitation [25] give the value of remanence ratio 0.27 at room temperature, whereas 13-nm cobalt ferrite NPs prepared by the polymeric precursor method [24] give the value of remanence ratio 0.5 for similar conditions. Moreover, 39 nm particles made by thermal method found the remanence ratio 0.407 [27]. It has been reported that for particles having $R < 0.5$ interact by magnetostatic interaction, while $R = 0.5$ is for randomly oriented noninteracting particles that undergo coherent rotations [28, 29]. Therefore, in this research the value of R lower than 0.5 is attributed to particles that interact by magnetostatic interactions.

3.6 Electrical properties

3.6.1 AC conductivity

To understand the conduction mechanism, the variation of AC conductivity with frequency at different temperatures is shown in Fig. 6. It is seen that at room temperature the AC conductivity increases with the increase of frequency. This can be explained using Koop's dispersion relations based on the Maxwell–Wagner model [8] considering inhomogeneous double layer dielectric structure. The grains with high conductivity are formed during the ferrite preparation. These
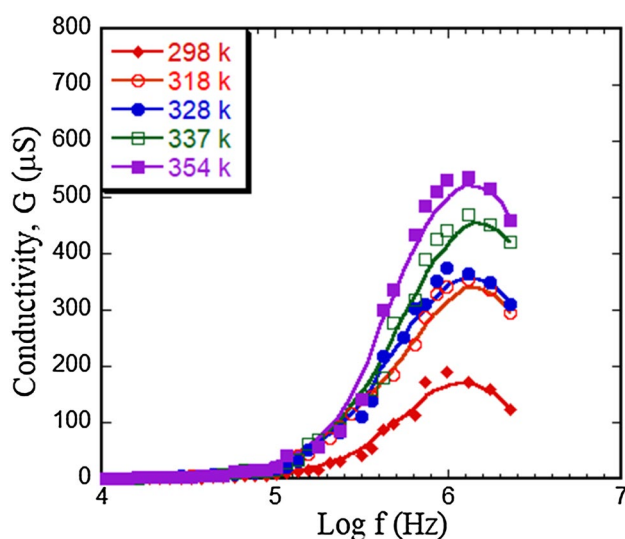

Fig. 6 The variation of AC conductivity as a function of frequency at different temperatures

grains are separated by poorly conducting grain boundaries. As the frequency of applied field increases, conducting grains more active and the hopping between the Fe^{2+} and the Fe^{3+} ions enhances which causes an increase in the mobility of charge carriers, resulting the increase of conductivity. Moreover, it is noticed that increasing the temperature the conductivity is also increased. This increase in conductivity with temperature is assumed due to the increase of drift mobility of the charge carriers thereby enhancing the charge hopping. However, at higher frequencies conductivity is less temperature dependent due to the hopping ions could not follow the applied frequency and the conductivity decreases at higher frequencies. In recent past, studies of the electrical conduction of a series of ferrites $Co_{1-x}Fe_{2+x}O_4$ were performed and reported the conductivity of ferrites resulting from hopping of holes between Co^{2+} and Co^{3+} ions and hopping of electrons between Fe^{2+} and Fe^{3+} ions [7]. Thus, the predominant conduction mechanism in spinel cobalt ferrite can be summarized as follows: $Co^{2+} + Fe^{3+} \leftrightarrow Co^{3+} + Fe^{2+}$.

3.6.2 Dielectric properties

The dielectric properties of materials are affected by synthesis technique, temperature, the percentage of composition, density, crystal structure, porosity and heat treatment etc [30, 31]. The dielectric constant (ε'), ($\varepsilon' = Cd/\varepsilon_o A$, where, C is the capacitance, d is the thickness of the disk, A is the cross-sectional area and ε_o is the permittivity of the free space) and loss factor (tan δ) as a function of frequency of the as synthesized NPs annealed at 600 °C are illustrated in Fig. 7. In an AC field, the dielectric constant is a complex quantity and we have measured the real part of this quantity as a function of frequency. It is observed (Fig. 7a) that at room temperature the value of ε' is higher at low frequencies and the dielectric constant decreases rapidly with increasing the frequency. Moreover, the dielectric constant possesses low values at temperatures 318 K, 328 K, 337 K and 354 K (inset), which is also decreased with the increasing of frequency. This is due to change of cationic states as mentioned in Sect. 3.6.1 and interfacial polarization which can be explained by Maxwell–Wagner model [8]. In this model, the dielectric materials are assumed to be composed of conducting grains separated by poorly conducting grain boundaries. The poorly conducing grain boundaries have been found to be effective at lower frequencies while at higher frequencies conducting grains is fairly effective. Moreover, the mechanism of polarization in polycrystalline ferrite can be explained through the hopping of electrons between ions of the same element in different oxidation states at tetrahedral site [32]. When a field is applied, the electron flow in the direction of the field within the grain through hopping and pile up at the grain boundaries to produce polarization. If the frequency of the field increases, the electron cannot follow the applied field, i.e., electron changes their direction as well as decreases the
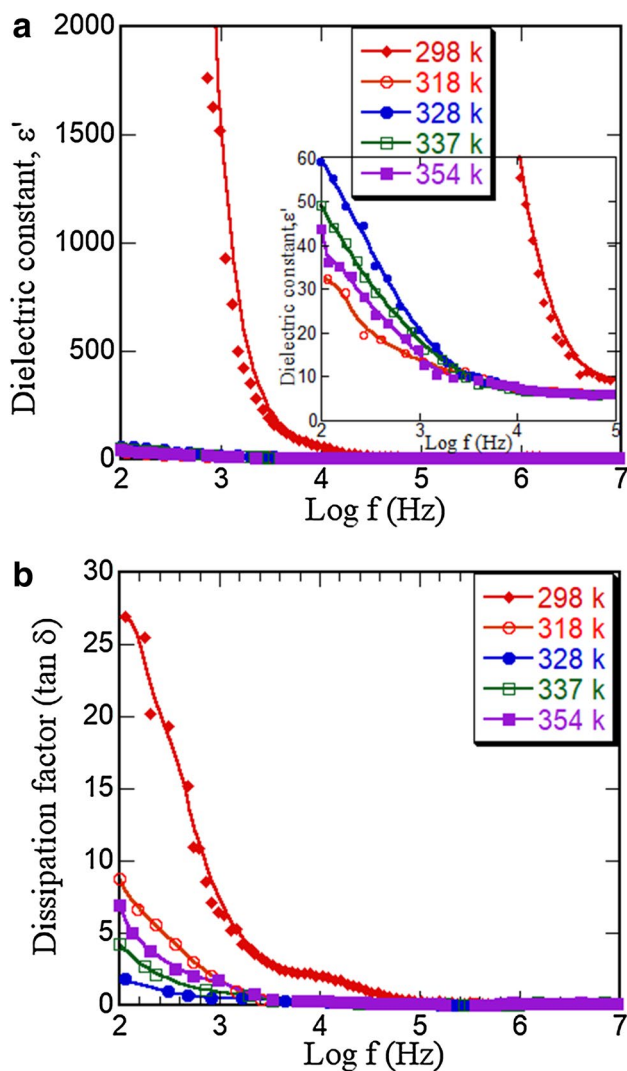
Fig. 7 Variation of **a** dielectric constant (inset for better clarity of data points) and **b** dissipation factor with frequency at different temperatures

probability of electrons to reach the grain boundaries. Thus, the polarization and dielectric constant decreases [12].

The dissipation factor ($\tan\delta = \varepsilon''/\varepsilon'$, where ε' is the real part of the permittivity and ε'' is the imaginary part of the permittivity) is illustrated in Fig. 7b. It is seen that the loss tangent decreases with the increasing of frequency and in the high frequency region it is nearly zero. The low values of loss tangent indicate the low eddy loss of current [12, 20].

4 Conclusion

The cobalt ferrite nanoparticles have been synthesized using citrate assisted sol gel route. The 17.5% porosity, which we found in synthesized NPs plays an important role in technological applications, e.g., water and chemical filtration related to bio-medical applications, materials science, etc. The phase transition temperature and thermal stability over a wide range of temperature have been investigated through the TGA and DTA curves. Magnetization measurement reveals that the synthesized NPs are soft ferrimagnetic with low coercivity and high saturation magnetization of single domain particles. The AC conductivity of the NPs confirms the mobility increases with frequency resulting to the hopping of electrons. The low dielectric constant and dissipation factor are found in the synthesized $CoFe_2O_4$ NPs. This low dielectric constant and low dissipation factor of the NPs indicate the low eddy loss in the system, which makes the $CoFe_2O_4$ NPs as a promising tool for high frequency applications.

References

1. G.E. Fish, Proc. IEEE, **78**, 947 (1990)
2. T. Abraham, JOM, 16 (1995)
3. N. Spaldin, *Magnetic Materials* (Cambridge University Press, Cambridge, 2003)
4. P.C. Rajath, R.S. Manna, D. Banerjee, M.R. Varma, K.G. Suresh, A.K. Nigam, J. Alloys Compd. **453**, 298 (2008)
5. M.S. Khandekar, R.C. Kamble, J.Y. Patil, Y.D. Kolekar, S.S. Suryavanshi, J. Alloys Compd. **509**, 1861 (2011)
6. N.M. Deraz, J. Anal. Appl. Pyrolysis **88**, 103 (2010)
7. G.H. Jonker, J. Phys. Chem. Solids **9**, 165 (1959)
8. K.W. Wagner, Ann. Phys. **40**, 317 (1973)
9. M. Sajjia, M. Oubaha, M. Hasanuzzaman, A.G. Olabi, Ceram. Int. **40**, 1147 (2014)
10. P. Laokul, S. Arthan, S. Maensiri, E. Swatsitang, J Supercond. Nov. Magn. **28**, 2483 (2015)
11. P.C. Morais, V.K. Garg, A.C. Oliveira, L.P. Silva, R.B. Azevedo, A.M.L. Silva, E.C.D. Lima, J. Magn. Magn. Mater. **225**, 37 (2004)
12. M. Amal, M.M. Ibrahim, M.M. Abd El-Latif, Mahmoud, J. Alloys Compd. **506**, 201 (2010)
13. P. Scherrer, Göttinger Nachrichten Gesell. **2**, 98 (1918)
14. Y.H. Hou, Y.J. Zhao, Z.W. Liu, H.Y. Yu, X.C. Zhong, W.Q. Qiu, D.C. Zengand, L.S. Wen, J. Phys. D Appl. Phys. **43**, 445003 (2010)
15. Ch Turquat, Ch Leroux, A. Gloter, V. Serin, G. Nihoul, I. J. Inorg. Mater. **3**, 1025 (2001)
16. L. Zhao, H. Zhang, Y. Xing, S. Song, S. Yu, W. Shi, X. Guo, J. Yang, Y. Lei, F. Cao, J. Solid State Chem. **181**, 245 (2008)
17. S.S. Rana, J.J. Philip, B. Raj, Mater. Chem. Phys. **124**, 264 (2010)
18. K.K. Senapati, C. Borgohain, P. Phukan, J. Mol. Catal. A Chem. **339**, 24 (2011)
19. S. Farhadi, J. Safabakhsh, P. Zaringhadam, J. Nanostructure Chem. **3**, 69 (2013)

20. A. Gatelyte, D. Jasaitis, A. Beganskiene, A. Kareiva, Mater. Sci. **17**, 3 (2011)
21. A.L. Andrade, D.M. Souza, M.C. Pereira, J.D. Fabris, R.Z. Domingues, Ceramica **55**, 420 (2009)
22. K. Zhang, O. Amponsah, M. Arslan, T. Holloway, W. Cao, A.K. Pradhan, J. Appl. Phys. **111**, 07B525 (2012)
23. Y. Zhang, Y. Liu, C. Fei, Z. Yang, Z. Lu et al., J. Appl. Phys. **108**, 084312 (2010)
24. D.S. Mathew, R.S. Juang, Chem. Eng. J. **29**, 51 (2007)
25. Y. Qu, H. Yang, N. Yang, Y. Fan, H. Zhu, G. Zou, Mater. Lett. **60**, 3548 (2006)
26. M. Gharagozlou, J. Alloys Compd. **486**, 660 (2009)
27. M.G. Naseri, E.B. Saion, H.A. Ahangar, A.H. Shaari, M. Hashim, J. Nanomater. 2010 (2010) (**article ID: 907686**)
28. Z.L. Wang, Y. Liu, Z. Zhang, *Materials Systems and Applications I*, vol. III (Kluwer Academic, Boston, Mass, USA, 2003) (**Plenum, New York**)
29. E.C. Stoner, E.P. Wohlfarth, Philos. Trans. R. Soc. Lond. **240**, 599 (1948)
30. M. Ma, Y. Wu, J. Zhou, Y. Sun, Y. Zhang, N. Gu, J. Magn. Magn. Mater. **268**, 33 (2004)
31. S.E. Shirsath, B.G. Toksha, K.M. Jadhav, Mater. Chem. Phys. **117**, 163 (2009)
32. M.C. Dimri, A. Verma, S.C. Kashyap, D.C. Dube, O.P. Thakur, C. Prakash, Mater. Sci. Eng. B **42**, 133 (2006)